HOKKAIDO UNIVERSITY

Title	A Novel Technique for Controlling Anisotropic Ion Diffusion : Bulk Single-Crystalline Metallic Silicon Clathrate
Author(s)	Iwasaki, Suguru; Morito, Haruhiko; Komine, Takashi; Morita, Kazuki; Shibuya, Taizo; Nishii, Junji; Fujioka, Masaya
Citation	Advanced Materials, 34(9), 2106754 https://doi.org/10.1002/adma.202106754
Issue Date	2022-03-03
Doc URL	http://hdl.handle.net/2115/88651
Rights	This is the peer reviewed version of the following article: [Iwasaki, S., Morito, H., Komine, T., Morita, K., Shibuya, T., Nishii, J., Fujioka, M., A Novel Technique for Controlling Anisotropic Ion Diffusion: Bulk Single-Crystalline Metallic Silicon Clathrate. Adv. Mater. 2022, 34, 2106754. https://doi.org/10.1002/adma.202106754], which has been published in final form at https://doi.org/10.1002/adma.202106754. This article may be used for non-commercial purposes in accordance with Wiley Terms and Conditions for Use of Self-Archived Versions. This article may not be enhanced, enriched or otherwise transformed into a derivative work, without express permission from Wiley or by statutory rights under applicable legislation. Copyright notices must not be removed, obscured or modified. The article must be linked to Wiley ’ s version of record on Wiley Online Library and any embedding, framing or otherwise making available the article or pages thereof by third parties from platforms, services and websites other than Wiley Online Library must be prohibited.
Type	article (author version)
File Information	production data.pdf

Instructions for use

Hokkaido University Collection of Scholarly and Academic Papers : HUSCAP

Novel technique for controlling anisotropic ion diffusion: bulk single-crystalline metallic silicon clathrate

Suguru Iwasaki[1], Haruhiko Morito[2], Takashi Komine[3], Kazuki Morita[4], Taizo Shibuya[5], Junji Nishii[1], Masaya Fujioka[1]*

[1] Research Institute for Electronic Science, Hokkaido University, Kita 20, Nishi 10, Kita-ku, Sapporo 001-0020, Japan

[2] Institute for Materials Research, Tohoku University, 2-1-1 Katahira, Aoba-ku, Sendai 980-8577, Japan.

[3] Graduate School of Science and Engineering, Ibaraki University, 4-12-1 Nakanarusawa, Hitachi, Ibaraki 316-8511, Japan

[4] Department of Materials, Imperial College London, London SW7 2AZ, United Kingdom

[5] System Platform Research Laboratories, NEC Corporation, 1753 Shimonumabe, Nakahara, Kawasaki 211-8666, Japan

E-mail: fujioka@es.hokudai.ac.jp

Keywords: anisotropic diffusion control of ions, metastable phase, type-II silicon clathrate, $Na_{24}Si_{136}$, deintercalation

Abstract

Na-free Si clathrates consisting only of Si cages are an allotrope of diamond-structured Si. This material is promising for various device applications, such as next-generation photovoltaics. The probable technique for synthesizing Na-free Si clathrates is to extract Na^+ from the Si cages of $Na_{24}Si_{136}$. Vacuum annealing is presently a well-known conventional and effective approach for extracting Na. However, this study demonstrates that Na^+ cannot be extracted from the surface of a single-crystalline type-II metallic Si clathrate ($Na_{24}Si_{136}$) in areas deeper than 150 μm. Therefore, a novel method was developed to control anisotropic ion diffusion: this is effective for various compounds with a large difference in the bonding strength between their constituent elements, such as $Na_{24}Si_{136}$ composed of covalent Si cages and weakly trapped Na^+. By skillfully exploiting the difference in the chemical potentials as a driving force, Na^+ was homogeneously extracted regardless of the size of the single crystal while maintaining high crystallinity. Additionally, the proposed point defect model was evaluated via density functional theory (DFT), and the migration of Na^+ between the Si cages was explained. It is expected that the developed experimental and computational techniques would significantly advance material design for synthesizing thermodynamically metastable materials.

1. Introduction

Si is the second most abundant element in the Earth's crust, after oxygen; it exhibits several allotropes, such as diamond-structured Si (d-Si), 2D-structured silicene,[1] guest-free tunnel-structured Si_{24},[2] and guest-free Si clathrate.[3] Among them, d-Si has contributed greatly to the advancement of the semiconductor industry and is an established core material for manufacturing semiconductors. Another allotrope of Si, guest-free Si clathrate (comprising only Si cages), is a promising material in various device applications, such as photovoltaics,[4] electrode materials for ion batteries,[5] and hydrogen-gas storage,[6] owing to its optical properties and unique crystal structures. Particularly, Si clathrate with a direct band gap has the potential to significantly improve the energy-conversion efficiencies of commercial solar cells employing d-Si with an indirect band gap. However, owing to thermodynamic limitations, it is challenging to directly synthesize only Si clathrates without the guest ions. Hence, the following two-step process has been employed as the synthetic route toward guest-free Si clathrates: the preparation of Na-intercalated Si clathrates, followed by the extraction of Na^+ from the Si cages while maintaining the cage structure. For the device application of guest-free Si clathrates, a sizable single crystal is required; thus, two significant challenges must be overcome: (i) the growth of a single crystal of the Na-intercalated Si clathrate that is sufficiently large for the applications and (ii) the removal of the Na^+ from such a sizable single crystal.

Furthermore, experimentally obtained Na-intercalated Si clathrates are primarily classified as type-I and type-II structures.[3] Type-I Si clathrates comprise two dodecahedrons (Si_{20} cages) and six tetrakaidecahedrons (Si_{24} cages), whereas type-II Si clathrates comprise 16 dodecahedrons (Si_{20} cages) and eight hexakaidecahedrons (Si_{28} cages), as shown in **Figure 1**(a).[7] When Na^+ occupies all the cages separately, the chemical formulas of type-I and type-II clathrates would be expressed as Na_8Si_{46} and $Na_{24}Si_{136}$, respectively. Regarding these two types of Si clathrates, the extraction of Na from Na_8Si_{46} exhibiting a type-I structure has never been reported, whereas the type-II Si clathrates exhibit a non-stoichiometric feature of Na^+.[8–17] Here, type-II $Na_{24}Si_{136}$, which is a promising candidate for synthesizing guest-free Si clathrates as a precursor, was focused on.

First, the employed crystal growth techniques for synthesizing $Na_{24}Si_{136}$ are overviewed. Conventionally, the thermal decomposition of NaSi has been employed to synthesize Na-intercalated Si clathrates as a powdery crystal. In 2011, Stefanoski *et al*. reported the synthesis of a $Na_{24}Si_{136}$ single crystal (~300 μm) via spark plasma sintering.[18] Yamanaka *et al.*[9] employed a high-pressure technique to synthesize Na-intercalated Si clathrates. The resulting products formed clusters of crystals with domain sizes of hundreds of micrometers. In 2016, Morito *et al*. reported the single-crystal growth of $Na_{24}Si_{136}$ (single domain size > 1 mm) via the evaporation of Na from a Na–Si–Sn solution: this method is known as the Na–Sn flux method.[19] Based on the intense desire to grow larger single crystals, this method could achieve the growth of crystals that are > 3 mm.[20] A further enlargement of the crystal size can be achieved via efficient crystal growth methods, such as the crystal pulling and top-seeded methods, employing seed crystals; these can be further advanced in the future.

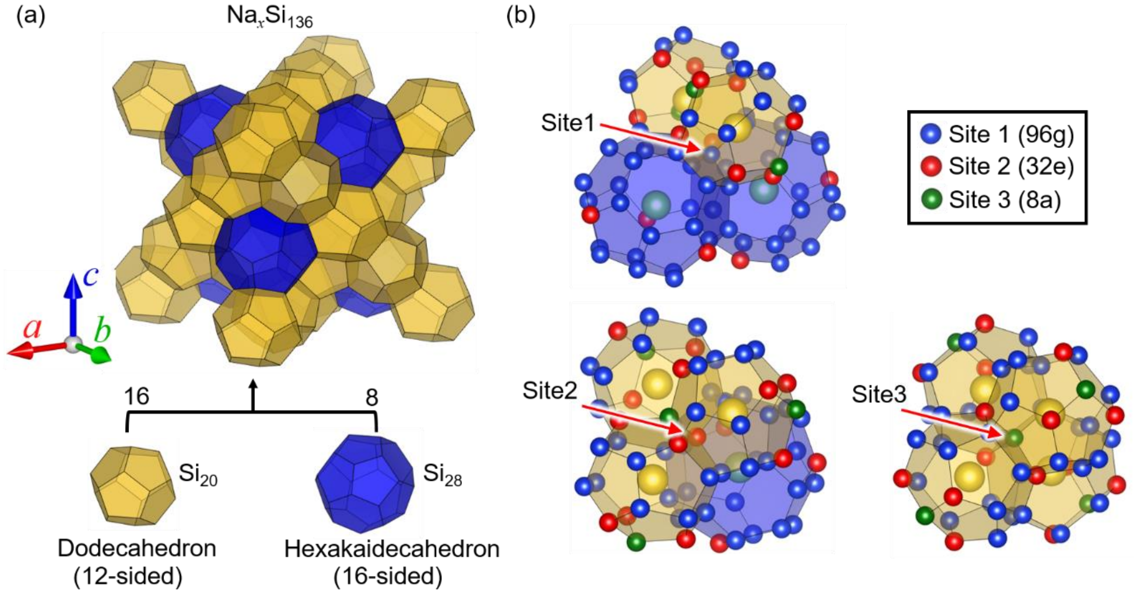

Figure 1. (a) Crystal structure of Na$_x$Si$_{136}$ (type-II Si clathrate). The crystal system is cubic, and the space group is Fd$\bar{3}$m (No. 227). Type-II Si clathrates consist of 16 Si$_{20}$ cages and eight Si$_{28}$ cages. (b) Four cages around a Si atom at Site 1 (96g), Site 2 (32e), and Site 3 (8a). Each Si atom at Site 1, 2, and 3 is shared by four cages: "Si$_{28}$ × 2 and Si$_{20}$ × 2," "a Si$_{28}$ and Si$_{20}$ × 3," and "Si$_{20}$ × 4," respectively. The crystal structures were drawn with VESTA.[7]

The second key technology involves the extraction of Na$^+$ from the Si cage structure. Vacuum annealing has been conventionally employed as an effective method for extracting Na from powdery crystals. Gryko *et al.* cycled vacuum annealing and HCl washing until no more Na was extracted.[11] The resulting product exhibited $x = 0.1$, where x is the amount of Na in Na$_x$Si$_{136}$, and its band gap, as estimated via optical absorption measurements, was 1.9 eV. Afterward, Himeno *et al.*[12] and Moriguchi *et al.*[21] determined that the band gap of 1.9 eV corresponded to a direct type. To extract additional Na ions, Ammar *et al*. performed annealing under iodine pressure, following repeated vacuum annealing and acid washing.[8] This process yielded Na-deintercalated Na_xSi_{136} ($x = 0.0058$). Additionally, Stefanoski *et al*. controlled the Na content to $x = 2.9$ by applying a heat treatment at 10 Torr in a nitrogen atmosphere and demonstrated that the metallic conductive property of $Na_{24}Si_{136}$ was changed into a semiconductive one by decreasing the Na concentration.[10]

In all these studies, Na extraction proceeded on samples comprising tiny crystallites of hundreds of micrometers. Although vacuum annealing effectively extracted Na^+ from such a powdery morphology, this study demonstrates that it was challenging to homogeneously extract Na^+ from the inside of large single crystals with domain sizes exceeding a few millimeters. Therefore, to achieve the homogeneous extraction of Na, a novel technique, which could replace vacuum annealing, was required.

To develop such a novel technique, synthetic technologies based on ion diffusion, such as alkali–proton substitution (APS),[22] corona discharge treatment (CDT),[23] and proton-driven ion introduction (PDII),[24] which had been developed by our group, were exploited. These techniques are effective for compounds composed of weakly bonded ions and robust frame structures and have the potential to achieve thermodynamically metastable phases by diffusing only the weakly bonded ions while maintaining the frame structure. $Na_{24}Si_{136}$ is one of such compounds because of its covalent Si cage structure in which Na^+ are weakly trapped.

The most challenging aspect of extracting Na^+ from $Na_{24}Si_{136}$ is that an electric field cannot be applied as a driving force because of electrostatic shielding. Therefore, we skillfully utilized the difference in the chemical potential as a driving force for extracting Na. This concept ensures the control of anisotropic ion diffusion, even for metallic compounds, and is expected to expose new exploration areas for thermodynamically metastable materials.

2. Results and discussion

2.1 Extraction of Na

Na^+ was extracted from $Na_{24}Si_{136}$ via anisotropic diffusion control (ADC), as experimentally shown in **Figure 2**(a) and (b). A single crystal of $Na_{24}Si_{136}$ was placed on a 1100 °C preannealed[25] $Na_3Zr_2Si_2PO_{12}$ pellet, which is known as a Na superionic conductor (NASICON). The single crystal and $Na_3Zr_2Si_2PO_{12}$ pellet were sandwiched in the SUS anode and graphite cathode. Additionally, a flexible graphite sheet (NeoGraf, Grafoil) was inserted between the sample and the SUS anode. This SUS anode/graphite/$Na_{24}Si_{136}$/$Na_3Zr_2Si_2PO_{12}$/graphite cathode composite was fixed between alumina plates. The electrical circuit was built according to this setup, as indicated by the red and blue lines in Figure 2(a).

Figure 2(d)–(i) show the optical images of the Na-removed samples that were obtained via ADC with V = 50 and 0 V, as well as vacuum annealing. The ADC process with the applied voltage maintained the purity of the sample surface without any contamination during the treatment; further, no crack was observed. Conversely, the sample, which was subjected to a vacuum annealing treatment, exhibited a large crack and was almost fully covered by a white impurity. Energy-dispersive X-ray spectroscopy (EDS) analysis revealed that the main component of the white impurity was Na_2CO_3, which accrued from the volatilized Na. Similarly, Figure 2(f) shows that a white impurity was observed on the surface of the sample that was annealed employing the ADC setup without an applied voltage, indicating that Na^+ could be released from the surface regardless of the atmospheric pressure of the N_2 carrier gas. Although the samples in Figure 2(d) and (f) were treated in the same environment (except for the application or nonapplication of the applied voltage), the former did not exhibit any impurity on its surface. Thus, the application of 50 V contributed to the suppression of the volatilization of Na and induced different surface conditions.

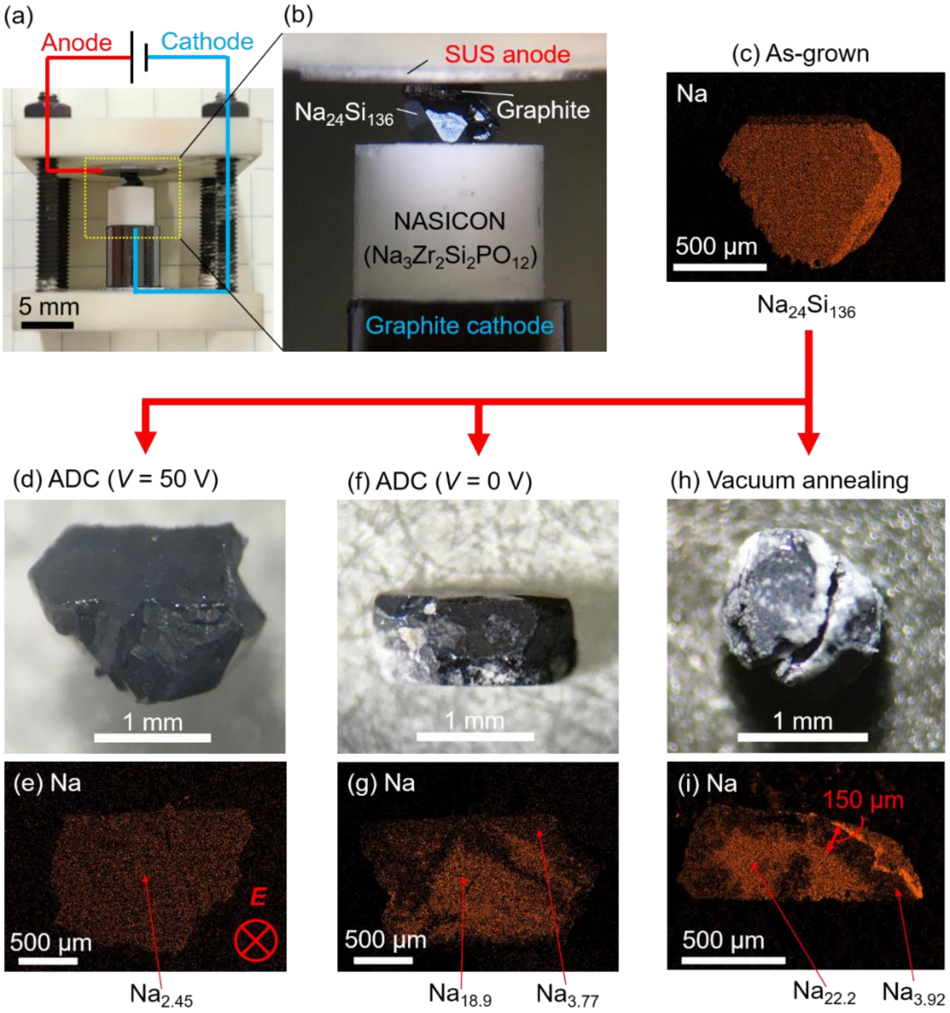

Figure 2. (a) Overall view of the experimental setup of the ADC process. The anode and cathode sides are represented by the red and blue lines, respectively. (b) Magnified view of (a) between the SUS anode and the graphite cathode. (c) EDS mapping of Na for the as-grown $Na_{24}Si_{136}$ single crystal. (d–i) Optical images and EDS mappings of Na for the Na_xSi_{136} samples that were obtained via (d and e) ADC with V = 50 V (the direction of the applied electric field is indicated), (f and g) ADC with V = 0 V, and (h and i) vacuum annealing. The amounts of Na in Na_xSi_{136} are indicated at the bottom.

The cross-sectional EDS mappings of Na for the as-grown sample is shown in Figure 2(c), and those for the three samples are shown in Figure 2(e), (g), and (i). Regarding ADC with an applied voltage of 50 V, Na^+ was homogeneously decreased to $x = 2.45$. To confirm the three-dimensional (3D) homogeneity of the Na distribution, the sample surface was gradually scraped along the depth direction, after which the cross-sectional planes were observed, as schematically shown in **Figure 3**. Na^+ was homogeneously distributed along each cross-sectional plane, and the amount of Na in Na_xSi_{136} was $x < 2.60$. The average Na amount among all the positions was 2.4(2). These results demonstrated that ADC with an applied voltage homogeneously extracted Na^+ from the large single crystal and recorded a low Na concentration.

Employing vacuum annealing, Na^+ was barely extracted from the areas that were deeper than 150 μm as shown in Figure 2(i). The amount of Na near the surface was as low as 3.92, but that in the center was 22.2. Averagely, vacuum annealing removed 45.0 at.% Na ions (calculated from Figure S1). Despite prolonging the vacuum annealing treatment time, it was challenging to achieve the homogeneous extraction of Na^+ from the sample because the treatments for 8 and 3 days exhibited almost comparable results

(Figure S2). Therefore, the extraction of Na attained saturation after vacuum annealing for 3 days. Figure S3 shows that this inhomogeneous removal of Na^+ did not improve even when the sample was subjected to a higher vacuum annealing treatment (3.8×10^{-6} Torr).

Additionally, it was observed that annealing within the ADC setup could partially extract the Na^+ even without the applied voltage, as shown in Figure 2(g). The amount of Na near the anode side decreased to x = 3.77, whereas a large amount of Na (x = 18.9) remained in the other area. This result demonstrated that Na^+ were spontaneously removed when the sample was subjected to an ideal temperature and in contact with a Na-absorbing material, such as graphite. The driving force of this spontaneous Na^+ migration is suspected to be the difference between the chemical potentials of the clathrate and graphite at the boundary.

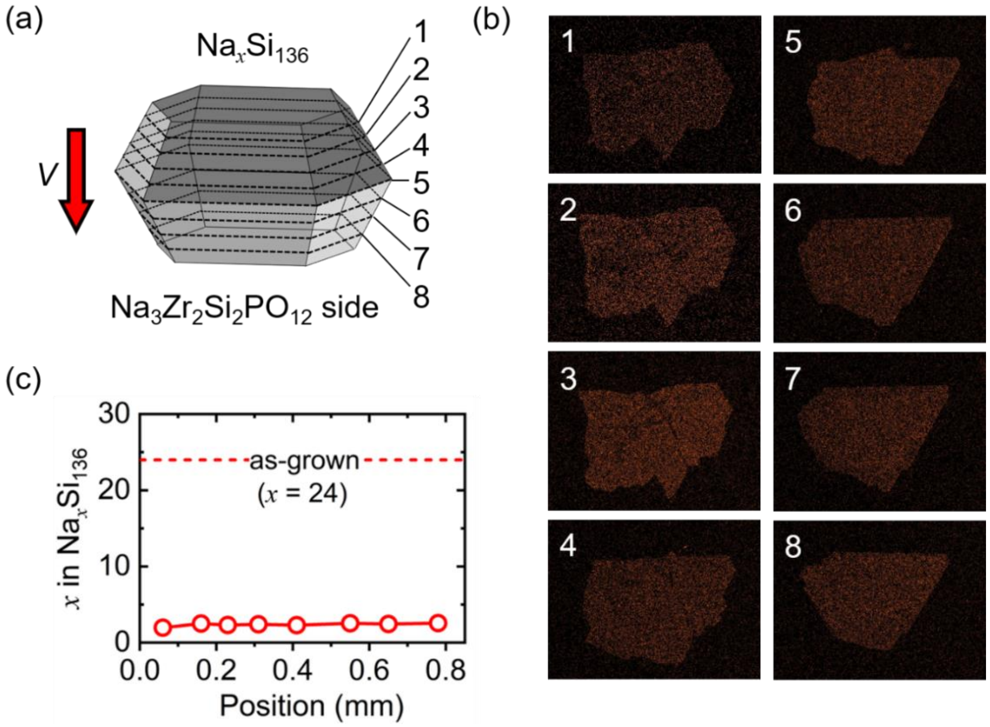

Figure 3. (a) Schematic illustration of the examined planes in a Na_xSi_{136} single crystal. (b) EDS mappings of Na in the cross-sectional area at each position indicated in (a). (c) Amount of Na in the ADC of Na_xSi_{136} at each position indicated in (a).

2.2 Effect of the applied voltage on the ADC process

Figure 4(a) shows the schematic illustration of the ADC setup. Since $Na_{24}Si_{136}$ exhibits a metallic transport property, it did not exhibit any voltage drop, indicating that the difference in the chemical potentials, rather than the electric field, was the driving force of Na migration from Na_xSi_{136} to $Na_3Zr_2Si_2PO_{12}$, as mentioned in section 2.1. Conversely, the applied voltage was mostly consumed by the electronically insulating $Na_3Zr_2Si_2PO_{12}$. Additionally, $Na_3Zr_2Si_2PO_{12}$ exhibits Na ionic conduction that was as high as ~0.41 S cm^{-1} at 450 °C.[26] Therefore, the electric field facilitated Na^+ migration toward the cathode side in $Na_3Zr_2Si_2PO_{12}$, thus inducing direct current (DC) polarization, which generated a Na-deficient area at the $Na_3Zr_2Si_2PO_{12}$–$Na_{24}Si_{136}$ interface. Figure 4(b) and (c) show the scanning electron microscopy (SEM)–EDS images of the surface and cross-section of this Na-deficient area in $Na_3Zr_2Si_2PO_{12}$. The Na concentration of the outermost surface was $y = 0.31$ in $Na_yZr_2Si_2PO_{12}$; it increased gradually to $y = 3$ at hundreds of micrometers away from the surface. Such a formation of the Na-deficient area should induce a significant difference in the chemical potentials at the interface with $Na_{24}Si_{136}$.

Herein, two different processes for the diffusion of Na (A and B in Figure 4(a)) were explored to clarify the mechanism of Na extraction. In diffusion process A, the interfacial Na-deficient area was formed via DC polarization that was derived from the applied voltage. In diffusion process B, the difference in the chemical potentials due to

Process A induced the migration of Na^+ in Na_xSi_{136} to the Na-deficient area in $Na_3Zr_2Si_2PO_{12}$. Therefore, as the applied voltage was retained at the Na-deficient area, Na^+ was released successively from the sizable single-crystalline Na_xSi_{136} with metallic properties until there was no difference in chemical potentials at the interface. This mechanism indicated that, as one of its notable features, the ADC process could homogeneously extract Na^+ regardless of the size of the single crystal and the effect of electrostatic shielding.

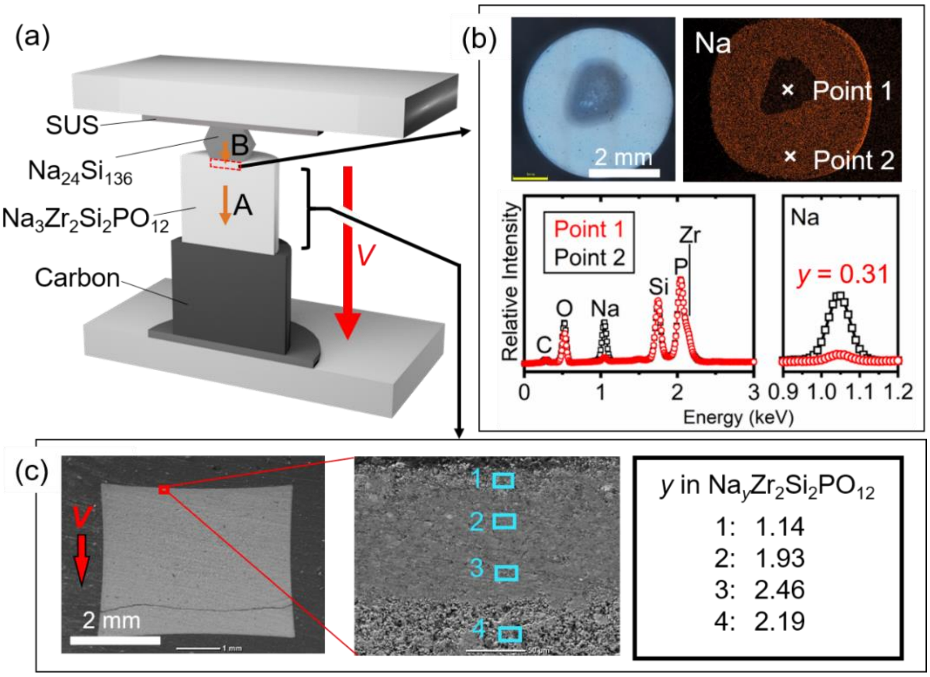

Figure 4. (a) Schematic illustration of the migration of Na via the ADC process. A: DC polarization of Na^+ in $Na_3Zr_2Si_2PO_{12}$ owing to the applied voltage. B: Thermal diffusion of Na^+ from $Na_{24}Si_{136}$ to the Na-deficient area owing to the difference in the chemical potentials. (b) Optical image, EDS mapping of Na, and the EDS spectra (red circles: point 1 on $Na_3Zr_2Si_2PO_{12}$ where Na_xSi_{136} was placed, black squares: point 2 on

$Na_3Zr_2Si_2PO_{12}$ where Na_xSi_{136} was not placed) of the $Na_3Zr_2Si_2PO_{12}$ pellet employed for ADC. The EDS spectra were normalized employing the area of the Si peaks. (c) Cross-sectional SEM image of the $Na_3Zr_2Si_2PO_{12}$ pellet. The quantitative analysis was performed in the 1, 2, 3, and 4 areas.

These diffusion processes of Na can elucidate the time dependence of the electrical current (I) during ADC (Figure S4). Figure S4(c) and (d) show that I did not flow even though a voltage of 50 V was applied at 20–25 °C. At ~300 °C, the Na^+ in $Na_3Zr_2Si_2PO_{12}$ started becoming biased, and a current peak appeared. Although the flow of I increased to 66 μA with the increasing temperature, it rapidly dropped to 1.5 μA because of the DC polarization in Process A between 0 and 15 h; afterward, it tended to decrease gradually in the subsequent hours in Process B. Since the diffusion of Na^+ from the Si cages is assumed to be the rate-determining step, the following reaction slowly progressed during Process A and B: $Na_xSi_{136} \rightarrow Na_{x-1}Si_{136} + Na^+ + e^-$. Based on this reaction, Na concentration gradually decreased with generating electrons. Consequently, as the difference in chemical potential decreased, the flow of Na^+ corresponding to I decreased, as shown in Figure S4(b).

Furthermore, the observed total electricity (Q) should be contributed by the following effects: the reaction for Na extraction (Q_{Na}), DC polarization (Q_{DC}), and the chemical reactions at interfaces (Q_{int}). Q_{DC} roughly corresponds to an area of the current peak in Process A in Figure S4(a). Additionally, Q_{Na} can be estimated from the Na concentration of the obtained products after ADC. When Na was extracted entirely from $Na_{24}Si_{136}$, the required electricity was estimated to be 0.9 C from the mass of the sample, the molar mass of $Na_{24}Si_{136}$, and Coulomb's constant. Also, the Na amount of the ADC-treated sample was x = 3.17 (Figure S5): the fraction of Na extracted was 0.87 (1 − (3.17/24)). Thus, the estimated Q_{Na} was 0.78 C (0.90 × 0.87). The contribution of Q_{Na} was exhibited as a highlighted area in purple in Figure S4(b) and occupied most of the area of Process B. Furthermore, its remaining area corresponded to Q_{int} and showed a shallow peak of I at around 50 h in Figure S4(b). As shown in Figure S6(e-h), this shallow peak was obviously grown up by applying a higher voltage of 100 V. This is suggested that the chemical reactions at the interfaces were accelerated by higher voltage. Thus the value of Q_{int} increases according to the applied voltage and is difficult to estimate directly, but it is possible to roughly grasp the progress of the Na extraction reaction from the behavior of I.

Figure S7 shows that the Na-deficient areas were not formed on $Na_3Zr_2Si_2PO_{12}$ when the voltage was not applied to the ADC process. Dissimilar to Figure 4(b), the Na concentration at the interface with $Na_{24}Si_{136}$ increased because of the volatilization of Na. In this case, the spontaneous extraction of Na would eventually stop, thus leaving many Na^+ in the single crystal. Furthermore, the sample surface was also covered by impurities, as shown in Figure 2(h). This result was almost the same even when a smaller single crystal with a diameter of ~1 mm was utilized. Since the total amount of Na was very small, its volatilization from the surface could ensure the extraction of Na^+ from the center of the single crystal; however, its surface was covered by Na-containing impurities, making the distribution of Na^+ inhomogeneous (Figure S8).

As previously mentioned, the application of the voltage was crucial to maintain the large difference in the chemical potentials at the interface by migrating the Na ions received from $Na_{24}Si_{136}$ to NASICON. Moreover, applying a higher voltage would contribute to a further decrease in Na^+ from Na-deficient area and a larger difference in the chemical potentials. However, such a decrease in the Na concentration would simultaneously promote the shrinkage of the lattice volume of the NASICON structure, thereby forming the weak contact of particles in the Na-deficient area and preventing Na^+ from diffusing. Figure S9 shows many fine clacks in the Na-deficient regions after ADC with 50 and 100 V, and a further decrease in Na concentration was confirmed by applying 100 V. Thus, the application of a higher voltage to NASICON could induce a more significant difference in the chemical potentials as a positive effect and weaken the intergrain contact as a negative effect; these two contradictory effects could be related to the final Na concentration of the product following ADC treatment. Figure S6(a-d) shows the evaluation of the resulting product that was treated by 100 V. Although the Na ions were homogeneously extracted, x in Na_xSi_{136} was 2.73, which was comparable to $x = 2.45$ in the 50 V case.

Therefore, substances that exhibit almost no change in their lattice volumes during ADC could be preferred to NASICON as candidates for ion-absorbing materials to advance the ADC process further.

2.3 Phase characterization and evaluation of electrical resistivity

Figure 5 (a) and (b) show the X-ray diffraction (XRD) patterns of the surfaces of the as-grown and (b) ADC-treated Na_xSi_{136}, respectively. The single crystal was placed such that the X-rays diffracted along the (111) planes. Obtained results indicated that the ADC process ensured the removal of Na^+ while maintaining the crystal structure of the Si clathrate. The peak positions of the ADC sample were shifted toward higher 2θ values when compared with those of the as-grown sample. This estimated lattice constant of the ADC sample was 1.4642(8) nm. This value is smaller than that

(1.4717(4) nm) of the as-grown sample. Figure S10 shows that the relationship between the shrinkage of the lattice constant and Na concentration agrees well with previous results.[9–11, 13, 14]

Figure 5(c) shows the dependence of the electrical resistivity (ρ) on the temperature (T) of the as-grown (black squares) and ADC-treated (red circles) samples of Na_xSi_{136} (x = 3.17). The details of sample characterization for the ADC-treated sample are shown in Figure S5. ρ of the as-grown $Na_{24}Si_{136}$ decreased with the decreasing T from 72 μΩ cm at 300 K to 2.0 μΩ cm at 5 K. Contrarily, ρ of the ADC-treated $Na_{3.17}Si_{136}$ increased with the decreasing T from 1.4 Ω cm at 300 K to 54 Ω cm at 5 K. Therefore, the metallic behavior could change into a semiconductive behavior owing to the deintercalation of Na. The resistivities obtained in this study were different from those of previously reported polycrystalline samples.[10] Regarding the as-grown sample $Na_{24}Si_{136}$, ρ of the single crystal was five times lower than that of the reported polycrystal at 300 K. This difference in ρ was likely caused by the grain boundaries. Conversely, the ADC-treated sample with x = 3.17 exhibited approximately 10 times higher resistivity than the reported polycrystalline sample with x = 2.9. A lower Na concentration would result in higher electrical resistance. Although the opposite results were obtained here, this difference was probably due to the limitations associated with estimating the internal Na concentration of the samples. Particularly, when vacuum annealing was employed, the Na^+ at the center of a domain was partially extracted, leaving residues, as mentioned above. The ADC treatment made little difference between the concentrations of the surface and interior.

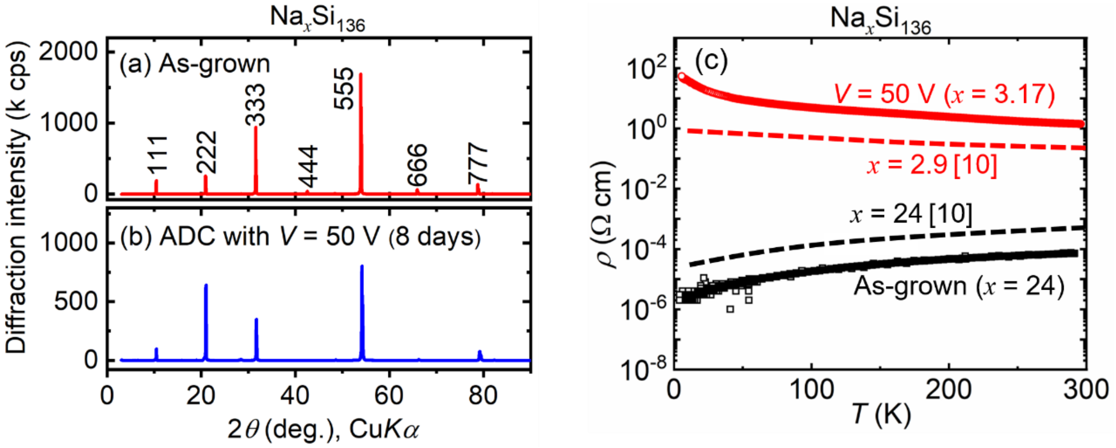

Figure 5. (a and b) XRD patterns of the (a) as-grown and (b) ADC-treated Na$_x$Si$_{136}$ samples. (c) Dependence of ρ on T of Na$_x$Si$_{136}$. The black squares and red circles indicate ρ of the as-grown and ADC-treated samples, respectively. The ρ–T curves of polycrystalline Na$_{24}$Si$_{136}$ and Na$_{2.9}$Si$_{136}$, which were reported by Stefanoski *et al.*,[10] are indicated by black and red dashed lines, respectively.

2.4 Diffusion mechanism of Na$^+$ in Na$_{24}$Si$_{136}$

The extraction of Na$^+$ from Na$_{24}$Si$_{136}$ proceeded via a thermal treatment at ~450 °C. However, the clathrate structure decomposed into a diamond one after thermal treatment at >450 °C. In this context, maintaining the temperature at 450 °C was crucial to promoting the diffusion of Na from Na$_{24}$Si$_{136}$ without decomposition. This also indicated that the thermal diffusion at 450 °C excited the Na$^+$ and induced their movements into adjacent cages beyond the activation energy (ΔG) for migration.

Si$_{28}$ and Si$_{20}$ cages are present in Na$_{24}$Si$_{136}$. The Si$_{20}$ cages comprise only pentagonal planes, whereas the Si$_{28}$ cages include hexagonal ones. Intuitively, the migration through the hexagonal plane is likely to exhibit a lower ΔG than that through the pentagonal plane because the hexagonal planes are larger. However, it was experimentally demonstrated that Na^+ in the Si_{20} cages consisting of only pentagonal planes were preferentially removed instead of those in the Si_{28} cages.[13, 15, 27] This contradiction between the expected ΔG and the experimental evidence has been controversial.

In this study, the nudged elastic band (NEB) method was employed to evaluate ΔG of the migration of Na. Generally, conducting ions can only migrate into vacant sites. Therefore, the migration of Na was modeled employing a unit cell of $Na_{23}Si_{136}$ with a Na-deficient cage. In this model, the following three pathways could be considered for the migration of Na: the migrations from Si_{28} into Si_{28}, Si_{28} into Si_{20} (or Si_{20} into Si_{28}), and Si_{20} into Si_{20}. Herein, these pathways are described as "Si_{28}–Si_{28}," "Si_{28}–Si_{20}," and "Si_{20}–Si_{20}," respectively. Figure S11 shows the crystal structures of the two adjacent cages that were related to the migration of Na and the results of ΔG obtained via the NEB calculations. In Paths Si_{28}–Si_{28} and Si_{20}–Si_{20} through the hexagonal (Figure S11(a)) and pentagonal (Figure S11(c)) planes, respectively, the estimated values of ΔG were 2.29 and 3.04 eV, respectively. The lowest value of ΔG (0.903 eV) was obtained when Na^+ migrated via the pentagonal plane of Si_{28}–Si_{20} (Figure S11(b)). However, a ΔG of 0.903 eV was still too high for a Na ion to exceed at 450 °C, as demonstrated in previous studies employing the Metropolis method[28]. Therefore, this model did not explain the migration of Na ions through the Si cages.

To explain the migration of Na, a novel model in which a point defect is considered was proposed. In a realistic scheme, the number of point defects in the compounds increases when T approaches their decomposition temperatures. In this study, the samples were annealed at 450 °C, which was nearly the maximum temperature required to avoid the decomposition of $Na_{24}Si_{136}$ into d-Si. When the point defects of Si in the cage structure are generated via a heat treatment at ~450 °C, these defects are expected to promote the migration of Na^+. Therefore, the migration of Na along a pathway with a point defect of Si was modeled employing the unit cell of $Na_{23}Si_{135}$. Notably, the legitimacy of this model was discussed by comparing the mechanism of ion diffusion in d-Si [29], as shown in Figure S12

Since each Si atom in type-II Si clathrates is shared by four Si cages, the introduction of a point defect of Si affects these cages (Figure 6 and Figure S13). Additionally, type-II Si clathrates exhibit three different sites (Sites 1, 2, and 3) for Si (Figure 1(b)). Further, each structure with a Si defect was constructed separately, and each ΔG along the path of the migration of Na was calculated.

The Si atom at Site 1 shares two Si_{28} and two Si_{20} cages. When a Si defect is introduced into Site 1, four possible paths through the Si defect can be considered: Si_{28}–Si_{28}, Si_{28}–Si_{20} (Path A), Si_{28}–Si_{20} (Path B), and Si_{20}–Si_{20}. Furthermore, two different paths are included in Si28–Si20: Paths A and B passing near the hexagonal and pentagonal planes, respectively (Figure S14). Similarly, the Si atom at Site 2 shares a Si_{28} and three Si_{20} cages; thus, there are two migration paths: Si_{28}–Si_{20} and Si_{20}–Si_{20}. Finally, the Si atom at Site 3 shares four Si_{20} cages; thus, Na^+ migrates between Si_{20}–Si_{20}. Overall, seven migration paths must be considered in the model with a defect in the Si cage.

Among them, the migration paths with the lowest and second-lowest ΔG values are shown in Figure 6. The lowest ΔG for the migration between Si_{20}–Si_{20} with a defect at Site 3 was 0.272 eV, and the second-lowest value was 0.320 eV between Si_{20}–Si_{20} with a defect at Site 1. These values were sufficiently low to induce the diffusion of Na^+

at 450 °C.[28] The migration paths and ΔG of the five other cases are shown in Figure S13, and the ΔG values in each case are summarized in Table 1.

Additionally, the formability of each defect site was discussed. The defect formation energy at Site 1 was 0.385 and 0.367 eV less than those of Sites 2 and 3, respectively. Therefore, the most dominant path of the migration of Na was Si_{20}–Si_{20} through the defect at Site 1. Thus, when the Si defect was considered in the migration of Na, it was unexpectedly observed that a lower ΔG value was obtained from the paths through a smaller pentagonal plane between Si_{20}–Si_{20}, indicating that Na^+ in the smaller Si_{20} cages were more easily extracted than those in the larger Si_{28} cages. These results demonstrated the experimental fact that Na^+ was preferentially extracted from a smaller Si_{20} cage.

Notably, this model, which introduces a single fixed point defect, is the simplest model for dealing with Si defects. To discuss more complicated and realistic situations, further extension of this model is necessary, such as considering the concentration and diffusion of defects using first-principles molecular dynamics.

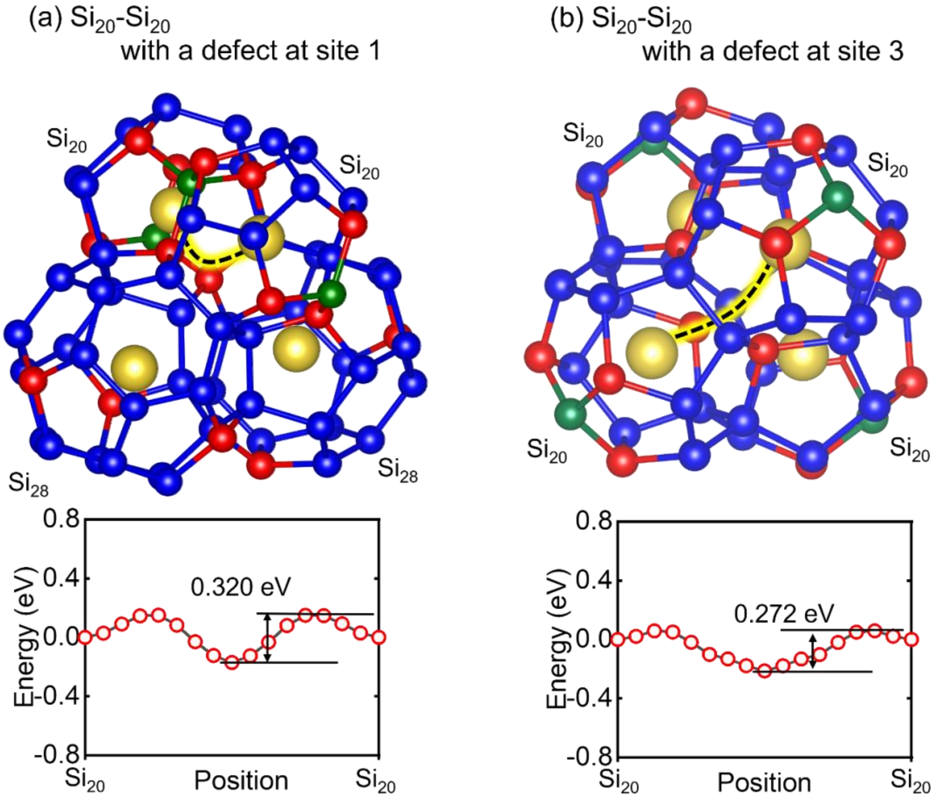

Figure 6. Two cases of the migrations between Si_{20}–Si_{20} in the model with Si defects at Sites (a) 1 and (b) 3. These cases exhibit the lowest and second-lowest Δ*G*s among the seven cases in the model exhibiting a defect. The other cases are shown in Figure S13. The migration paths are highlighted, and the energies along the migration paths are shown in the bottom figures. The crystal structures were drawn with VESTA.[7]

Table 1 Summary of the Δ*G*s.

No.	Defect site	Path	Δ*G* [eV]
1	No defect	Si_{28}–Si_{28}	2.29
2	No defect	Si_{28}–Si_{20}	0.903
3	No defect	Si_{20}–Si_{20}	3.04

4	Site 1 (96g)	Si_{28}–Si_{28}	0.604
5	Site 1 (96g)	Si_{28}–Si_{20} (Path A)	0.396
6	Site 1 (96g)	Si_{28}–Si_{20} (Path B)	0.457
7	Site 1 (96g)	Si_{20}–Si_{20}	0.320
8	Site 2 (32e)	Si_{28}–Si_{20}	0.832
9	Site 2 (32e)	Si_{20}–Si_{20}	0.553
10	Site 3 (8a)	Si_{20}–Si_{20}	0.272

2.5 Prospects of the ADC process toward metastable materials

In this study, ADC was employed to extract Na from $Na_{24}Si_{136}$. This method was developed based on the following two ideas, which can be generally applied to the syntheses of thermodynamically metastable materials.

1. Prolonged treatment in an optimum temperature range where only specific ion species can be diffused

ADC exploits the diffusion of only the specific ion in a solid compound. Such a diffusible ion must exhibit the weakest bonding state among the other constituents of the compounds, and the other elements must maintain a robust main structure regardless of the migration of the diffusible ions. Thus, the weaker the bond of the diffusible ions, the lower the temperature at which they can diffuse. For instance, a solid electrolyte that can be employed at room temperature comprises diffusible ions trapped with a low ΔG that can be excited at room temperature.

Figure 7 qualitatively shows the ΔG of Na and Si in $Na_{24}Si_{136}$. From the estimated ΔG of Na by our point defect model in section 2.4, heat treatment at several hundred degrees Celsius was required to excite it. When the treatment temperature was gradually increased, only Na^+ exceeded the ΔG at T_1 and began diffusing. Thereafter, a further increase in the temperature to T_2 induced the diffusion of Si and the decomposition of the clathrate structure into a more stable diamond one. Hence, it was possible to diffuse only Na^+ in the temperature range between T_1 and T_2. Notably, in the case of the liquid-phase process, the heat treatment temperature is limited by the evaporation of the solvent, but in the case of the all-solid-state process, it can be adjusted according to the target temperature; this will lead to a great expansion of the target substances for ADC.

Regarding $Na_{24}Si_{136}$, the samples were treated at the highest possible temperature near T_2 (450 °C); the diffusion capability of Na was maximized without structural decomposition. However, even at 450 °C, the current flowing through the circuit was only ~1 µA (Figure S4). Due to such a small ion conductivity, $Na_{24}Si_{136}$ might not be capable of functioning as a solid electrolyte for Na^+. However, from the viewpoint of inorganic material syntheses, the ability of high ion conductivity is not necessary for synthesizing thermodynamically metastable compounds. As demonstrated here, Na^+ could be extracted gradually over a prolonged processing period (one or more weeks) to achieve the homogeneous extraction of Na while maintaining the basic crystal structure and inducing a significant change in physical properties.

Among the compounds discovered thus far, there should be many compounds that are not known to exhibit slight ionic conductivity at high temperatures, such as $Na_{24}Si_{136}$. The prerequisite for applying the ADC to these compounds is that the bonding strengths between the diffusible elements and those responsible for the crystal structure must be sufficiently different. Finding such compounds and heat treating them in the temperature range of T_1–T_2 to diffuse the ions little by little over an extended period is expected to be one of the effective processes for synthesizing thermodynamically metastable compounds. Further, the established point defect model in this research was very consistent with experimental results. Such calculations might be employed as a guide for predicting their applicability to ADC and finding an appropriate processing temperature.

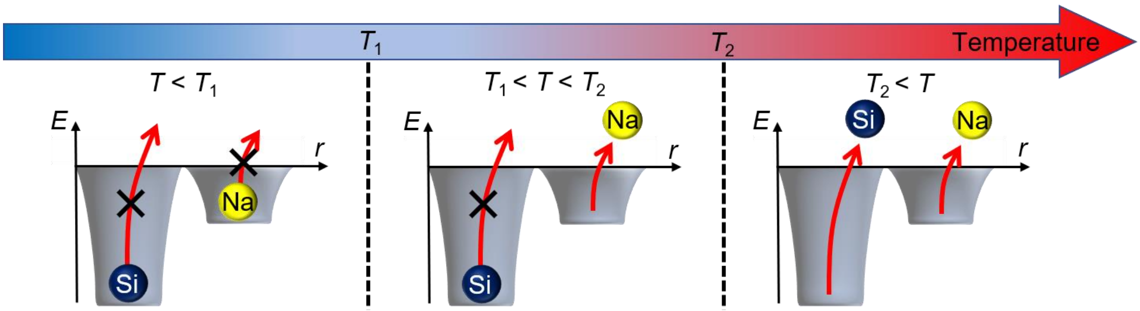

Figure 7. Relationship between *T* for diffusing ion species and its bonding state.

2. Ion diffusion in metallic materials that intentionally utilize the differences in chemical potentials

Even if the samples are treated in the T_1–T_2 temperature range, they would simply diffuse in all directions if no driving force is applied to the diffusible ions. The vacuum annealing (450 °C) in this study was closely similar to this phenomenon; thus, owing to thermal diffusion, Na^+-containing impurities were formed on the sample surface and suppressed its further diffusion (Figure 2(h)). To prevent this occurrence, a driving force was required to anisotropically diffuse Na^+. The application of voltage is the most common technique for controlling ion diffusion. However, regarding metallic materials, such as $Na_{24}Si_{136}$, an electric field is not possible to apply inside because of electrostatic shielding.

In this study, NASICON was placed at the bottom of the sample, and a voltage was applied to generate a Na-deficient area between NASICON and $Na_{24}Si_{136}$, thereby intentionally inducing a difference in the chemical potential as a driving force for extracting Na. This concept makes it possible to select the driving force based on the materials: an electric field and the chemical potential for insulating and metallic compounds, respectively. Such a materials design based on the above ideas (1 and 2) could advance developments regarding thermodynamically metastable materials. Particularly, controlling specific diffusible ions in metallic compounds exhibiting electrostatic shielding by applying appropriate driving force at proper temperatures is a field that has not been deeply investigated and must be advanced.

3. Conclusion

Guest-free Si clathrates exhibit promising applications in various next-generation devices. However, it is challenging to produce them as bulk bodies because they are thermodynamically metastable. This study demonstrated a synthesis strategy based on ADC, which focused on the extraction of Na from bulk single-crystalline Si clathrates. The key achievements of this study are summarized as follows: (i) a novel method based on ADC was demonstrated to obtain homogeneous Na-extracted bulk Na_xSi_{136} (x = 2.4), (ii) a reasonable point-defect model was established to explain the diffusion of Na in $Na_{24}Si_{136}$, and (iii) the fundamental ideas behind ADC for synthesizing thermodynamically metastable phase were reported.

First, the anisotropic ion diffusion process was developed and applied to the extraction of Na from $Na_{24}Si_{136}$. The Na^+ were homogeneously extracted from a sizable $Na_{24}Si_{136}$ single crystal while maintaining its high crystallinity, as well as not contaminating the surface. This method could be applied to much larger single crystals, which are expected to emerge as technology for the crystal growth of Na–Si clathrates develops in the future.

Second, a point defect model was established. Although a high treatment temperature excited Na^+ to exceed the ΔG for migration, the heat treatment at 450 °C was near the maximum temperature to prevent the structural change from clathrate to d-Si. Near the temperature for the structural change, the concentration of the Si defects should increase, promoting the migration of Na. Based on this insight, a point defect model for the migration of Na in type-II Si clathrates was proposed. This model indicated that the Si_{20}–Si_{20} path via a defect at Site 1 was the most dominant for the migration of Na. The calculations here indicated that the migration from Si_{20} was more probable than that from Si_{28} despite the smaller cage size of Si_{20}. These results could explain the experimentally observed selective extraction of Na from Si_{20}. Thus, the point defect model reasonably explained the previously unsolved paradox of Na migration.

Finally, the fundamental ideas behind ADC were discussed in section 2.5. Figure 7 shows that ADC targeted materials in which the difference between the bonding strengths of their constituent elements is large. The application of a certain driving force in the T_1–T_2 temperature range where specific ions are excited from its ΔG would allow only the anisotropic diffusion of the ions. In this study, the difference in the chemical potential was skillfully exploited for the successful extraction of Na^+ from the metallic compound regardless of electrostatic shielding. Conversely, depending on the situation, different driving forces, such as an electric field, a magnetic field, a chemical potential, a centrifugal force, and a strain force, could also be considered.

These findings would advance the materials design for the syntheses of metastable compounds. Furthermore, preferable compounds for ADC could be predicted if the bonding strength and activation energy of a mother compound can be accurately evaluated via computational studies. The developed point defect model will contribute to this computational prediction in the case of ADC at high temperatures because solid compounds near their melting point generally exhibit ion diffusion through defects.

4. Methods

4.1 Crystal growth of $Na_{24}Si_{136}$

The $Na_{24}Si_{136}$ single crystals were grown according to the methods in the literature.[19, 20] The raw materials, namely, a piece of Na metal (Nippon Soda, 99.95 wt.%), Si powder (Kojundo Chemical Laboratory, 99.99 wt.%), and Sn granules (Wako Pure Chemical Industries, 99.99 wt.%), were placed in a boron nitride crucible in a 6:2:1 molar ratio and sealed with a stainless-steel container in an Ar-filled glove box (O_2 and H_2O < 1 ppm). Thereafter, the container was heated for 12 h at 900 °C. Afterward, the obtained mixture was placed again in the boron nitride crucible and sealed with a stainless-steel container in an Ar-filled glove box, after which the container was heated for 9 h at 600 °C.

4.2 Removal of Na^+

For the ADC process, a voltage (V) of 50 V was applied between the anode and cathode, after which the composite was annealed at 450 °C[17] for 8 days in an N_2 flow. To clarify the function of the applied voltage in ADC, the composite was annealed at 450 °C for 8 days in an N_2 flow without applying the voltage ($V = 0$ V). Further, the

$Na_{24}Si_{136}$ single crystal was vacuum annealed for 8 days at 450 °C and 10^{-3} Torr to reveal the difference between ADC and conventional vacuum annealing.

4.3 Phase characterization and evaluation of electrical resistivity

The crystal phases of the as-grown and Na-extracted crystals were characterized via XRD (MiniFlex 600, Rigaku) exhibiting Cu Kα radiation. Elemental analysis was performed via EDS (MP-00040EDAD, Jeol) coupled with SEM (JCM-6000, Jeol). In each measurement, the peak area of Na was normalized employing that of Si. The actual amount of Na in Na_xSi_{136} was estimated from the ratio of the normalized Na peak areas between Na_xSi_{136} and $Na_{24}Si_{136}$. The dependence of ρ on T was measured between 4 and 300 K via the standard DC four-probe technique.

4.4 DFT calculations

The migration of Na^+ through the cage structure of the type-II Si clathrate was analyzed via DFT calculations employing the projector augmented-wave method in the Vienna *ab initio* simulation package.[30] The generalized gradient approximation (the Perdew, Burke, and Ernzerhof approximation[31]) was employed as the exchange-correlation functional. The structural relaxation of $Na_{24}Si_{136}$ was performed under the following conditions: the plane-wave cutoff energy was set to 400 eV, and a single k-point at (0, 0, 0) was used for the Brillouin zone sampling. Additionally, Gaussian smearing with $\sigma = 0.04$ was employed. The lattice parameters and ionic positions were relaxed until the Hellmann–Feynman forces were reduced to <0.03 eV $Å^{-1}$. The migration barriers of Na^+ were evaluated via the NEB method. To obtain the initial and final structures for NEB calculations, the ionic positions were relaxed by fixing the relaxed lattice parameters (14.770535 Å) of $Na_{24}Si_{136}$ and employing the above conditions.

Supporting Information

Supporting Information is available from the Wiley Online Library or from the author.

Acknowledgments

This work was supported by the Japan Science and Technology Agency (JST) CREST (Grant No. JPMJCR19J1), the Japan Society for the Promotion of Science (JSPS) (Grant No. 18H01887, 19H02420 and 20K22544), the Cooperative Research Programs of "Network Joint Research Center for Materials and Devices" and "the Dynamic Alliance for Open Innovation Bridging Human, Environment and Materials" and the GIMRT Program of the Institute for Materials Research, Tohoku University (Proposal No. 202012 RDKGE 0049).

Received: ((will be filled in by the editorial staff))
Revised: ((will be filled in by the editorial staff))
Published online: ((will be filled in by the editorial staff))

References

[1] P. Vogt, P. De Padova, C. Quaresima, J. Avila, E. Frantzeskakis, M. C. Asensio, A. Resta, B. Ealet, G. Le Lay, Physical Review Letters **2012**, 108, 155501.

[2] D. Y. Kim, S. Stefanoski, O. O. Kurakevych, T. A. Strobel, Nature Materials **2015**, 14, 169.

[3] J. S. Kasper, P. Hagenmuller, M. Pouchard, C. Cros, Science **1965**, 150, 1713; C. Cros, M. Pouchard, P. Hagenmuller, Journal of Solid State Chemistry **1970**, 2, 570; M. Pouchard, C. Cros, P. Hagenmuller, E. Reny, A. Ammar, M. Ménétrier, J.-M. Bassat, Solid State Sciences **2002**, 4, 723; C. Cros, M. Pouchard, Comptes Rendus Chimie **2009**, 12, 1014; M. Beekman, C. P. Sebastian, Y. Grin, G. S. Nolas, Journal of Electronic Materials **2009**, 38, 1136; S. Yamanaka, Dalton Transactions **2010**, 39, 1901; C. Cros, M. Pouchard, P. Hagenmuller, Compts Rendus de l'Académie des Sciences Paris **1965**, 260, 4764.

[4] A. D. Martinez, L. Krishna, L. L. Baranowski, M. T. Lusk, E. S. Toberer, A. C. Tamboli, IEEE Journal of Photovoltaics **2013**, 3, 1305; T. Kume, F. Ohashi, K. Sakai, A. Fukuyama, M. Imai, H. Udono, T. Ban, H. Habuchi, H. Suzuki, T. Ikari, S. Sasaki, S. Nonomura, Thin Solid Films **2016**, 609, 30; M. Yamaga, T. Kishita, K. Goto, S. Sunaba, T. Kume, T. Ban, R. Himeno, F. Ohashi, S. Nonomura, Journal of Physics and Chemistry of Solids **2020**, 140, 109358.

[5] J. Yang, J. S. Tse, Journal of Materials Chemistry A **2013**, 1, 7782; T. Langer, S. Dupke, H. Trill, S. Passerini, H. Eckert, R. Pöttgen, M. Winter, Journal of The Electrochemical Society **2012**, 159, A1318; N. A. Wagner, R. Raghavan, R. Zhao, Q. Wei, X. Peng, C. K. Chan, ChemElectroChem **2014**, 1, 347.

[6] D. Neiner, N. L. Okamoto, C. L. Condron, Q. M. Ramasse, P. Yu, N. D. Browning, S. M. Kauzlarich, Journal of the American Chemical Society **2007**, 129, 13857; D. Neiner, N. L. Okamoto, P. Yu, S. Leonard, C. L. Condron, M. F. Toney, Q. M. Ramasse, N. D. Browning, S. M. Kauzlarich, Inorganic Chemistry **2010**, 49, 815.

[7] K. Momma, F. Izumi, Journal of Applied Crystallography **2011**, 44, 1272.

[8] A. Ammar, C. Cros, M. Pouchard, N. Jaussaud, J.-M. Bassat, G. Villeneuve, M. Duttine, M. Ménétrier, E. Reny, Solid State Sciences **2004**, 6, 393.

[9] S. Yamanaka, M. Komatsu, M. Tanaka, H. Sawa, K. Inumaru, Journal of the American Chemical Society **2014**, 136, 7717.

[10] S. Stefanoski, C. D. Malliakas, M. G. Kanatzidis, G. S. Nolas, Inorganic Chemistry **2012**, 51, 8686.

[11] J. Gryko, F. M. Paul, F. M. Robert, K. R. Ganesh, P. Derek, K. D. Sudip, F. S. Otto, Physical Review B **2000**, 62, R7707.

[12] R. Himeno, F. Ohashi, T. Kume, E. Asai, T. Ban, T. Suzuki, T. Iida, H. Habuchi, Y. Tsutsumi, H. Natsuhara, S. Nonomura, Journal of Non-Crystalline Solids **2012**, 358, 2138; R. Himeno, T. Kume, F. Ohashi, T. Ban, S. Nonomura, Journal of Alloys and Compounds **2013**, 574, 398.

[13] G. K. Ramachandran, J. Dong, J. Diefenbacher, J. Gryko, R. F. Marzke, O. F. Sankey, P. F. McMillan, Journal of Solid State Chemistry **1999**, 145, 716; H.-O. Horie, T. Kikudome, K. Teramura, S. Yamanaka, Journal of Solid State Chemistry **2009**, 182, 129.

[14] E. Reny, P. Gravereau, C. Cros, M. Pouchard, Journal of Materials Chemistry **1998**, 8, 2839.

[15] L. Krishna, L. L. Baranowski, A. D. Martinez, C. A. Koh, P. C. Taylor, A. C. Tamboli, E. S. Toberer, CrystEngComm **2014**, 16, 3940.

[16] F. Tournus, B. Masenelli, P. Mélinon, D. Connétable, X. Blase, A. M. Flank, P. Lagarde, C. Cros, M. Pouchard, Physical Review B **2004**, 69, 035208.

[17] F. Ohashi, M. Hattori, T. Ogura, Y. Koketsu, R. Himeno, T. Kume, T. Ban, T. Iida, H. Habuchi, H. Natsuhara, S. Nonomura, Journal of Non-Crystalline Solids **2012**, 358, 2134.

[18] S. Stefanoski, M. Beekman, W. Wong-Ng, P. Zavalij, G. S. Nolas, Chemistry of Materials **2011**, 23, 1491.

[19] H. Morito, M. Shimoda, H. Yamane, Journal of Crystal Growth **2016**, 450, 164; H. Morito, M. Shimoda, H. Yamane, K. Fujiwara, Crystal Growth & Design **2017**, 18, 351.

[20] H. Morito, H. Yamane, R. Y. Umetsu, K. Fujiwara, Crystals **2021**, 11, 808.

[21] K. Moriguchi, S. Munetoh, A. Shintani, Physical Review B **2000**, 62, 7138.

[22] T. Ishiyama, S. Suzuki, J. Nishii, T. Yamashita, H. Kawazoe, T. Omata, Journal of The Electrochemical Society **2013**, 160, E143; T. Ishiyama, J. Nishii, T. Yamashita, H. Kawazoe, T. Omata, Journal of Materials Chemistry A **2014**, 2, 3940.

[23] T. Kinoshita, A. Miyazaki, K. Kawaguchi, D. Sakai, T. Yamaguchi, T. Omata, T. Ishiyama, M. Fujioka, H. Kaiju, J. Nishii, Applied Surface Science **2018**, 428, 718.

[24] M. Fujioka, C. Wu, N. Kubo, G. Zhao, A. Inoishi, S. Okada, S. Demura, H. Sakata, M. Ishimaru, H. Kaiju, J. Nishii, Journal of the American Chemical Society **2017**, 139, 17987; M. Fujioka, N. Kubo, M. Nagao, R. Msiska, N. Shirakawa, S. Demura, H. Sakata, H. Kaiju, J. Nishii, Journal of the Ceramic Society of Japan **2018**, 126, 963; K. Zagarzusem, M. Fujioka, T. Shibuya, S. Demura, S. Adachi, Y. Takano, M. Jeem, M. Ono, H. Kaiju, J. Nishii, 2D Materials **2020**, 8, 015007.

[25] A. Caneiro, P. Fabry, H. Khireddine, E. Siebert, Analytical Chemistry **1991**, 63, 2550.

[26] W. Baur, J. Dygas, D. Whitmore, J. Faber, Solid State Ionics **1986**, 18, 935.

[27] M. Beekman, E. N. Nenghabi, K. Biswas, C. W. Myles, M. Baitinger, Y. Grin, G. S. Nolas, Inorganic Chemistry **2010**, 49, 5338.

[28] K. Binder, D. W. Heermann, *Monte Carlo Simulation in Statistical Physics*, Springer, Berlin **2010**.

[29] H. Mehrer, *Diffusion in Solids*, Springer **2007**; V. V.Milman, M. C. Payne, V. V. Heine, R. J. Needs, J. S. Lin, M. H. Lee, Physical Review Letters **1993**, 70, 2928; L. Svob, Solid-State Electronics **1967**, 10, 991; M. N. Belikova, A. V. Zastavnyi, and V. M. Korol, Soviet Physics. Semiconducors. **1976**, 10, 319; J. O. McCaldin, Nuclear Instruments and Methods **1965**, 38, 153.

[30] G. Kresse, J. Furthmuller, Phys Rev B Condens Matter **1996**, 54, 11169; G. Kresse, J. Furthmüller, Computational Materials Science **1996**, 6, 15.

[31] J. P. Perdew, K. Burke, M. Ernzerhof, Physical Review Letters **1996**, 77, 3865.

Table of contents

Suguru Iwasaki[1], Haruhiko Morito[2], Takashi Komine[3], Kazuki Morita[4], Taizo Shibuya[5], Junji Nishii[1], Masaya Fujioka[1]*

Novel technique for controlling anisotropic ion diffusion: bulk single-crystalline metallic silicon clathrate

The anisotropic ion diffusion process was developed. This technique could homogeneously extract Na^+ from a type-II Si clathrate regardless of the size of the single crystal while maintaining high crystallinity by skillfully exploiting the difference in the chemical potentials as a driving force. The synthesis concept behind the technique is expected to expose new exploration areas for thermodynamically metastable materials.

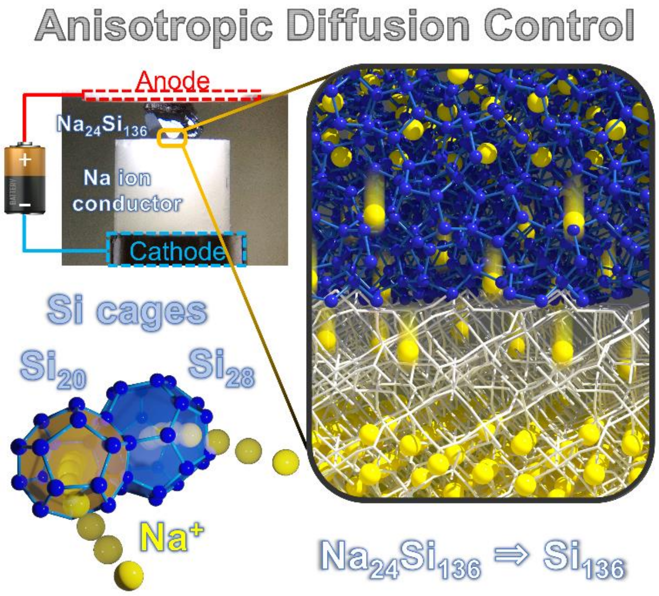

Supporting Information

Novel technique for controlling anisotropic ion diffusion: bulk single-crystalline metallic silicon clathrate

Suguru Iwasaki[1], Haruhiko Morito[2], Takashi Komine[3], Kazuki Morita[4], Taizo Shibuya[5], Junji Nishii[1], Masaya Fujioka[1]*

[1] Research Institute for Electronic Science, Hokkaido University, Kita 20, Nishi 10, Kita-ku, Sapporo 001-0020, Japan

[2] Institute for Materials Research, Tohoku University, 2-1-1 Katahira, Aoba-ku, Sendai 980-8577, Japan.

[3] Graduate School of Science and Engineering, Ibaraki University, 4-12-1 Nakanarusawa, Hitachi, Ibaraki 316-8511, Japan

[4] Department of Materials, Imperial College London, London SW7 2AZ, United Kingdom

[5] System Platform Research Laboratories, NEC Corporation, 1753 Shimonumabe, Nakahara, Kawasaki 211-8666, Japan

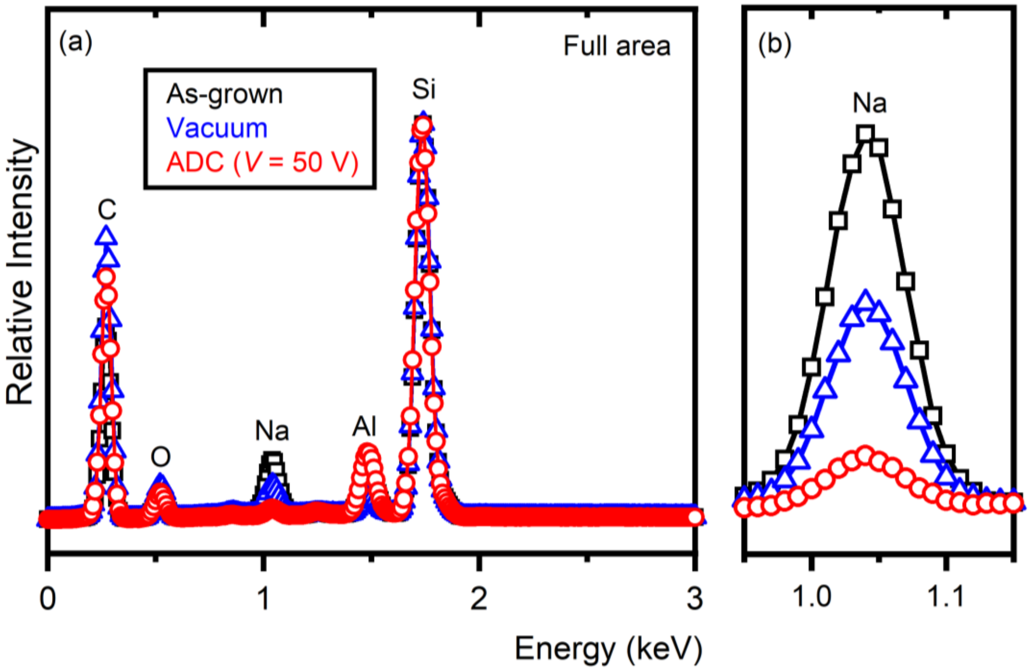

Figure S1. (a) Comparison of the energy dispersive X-ray spectroscopy (EDS) spectra of a full area in Figure 2(c), (e), and (i). Black squares: as-grown sample, blue triangles: vacuum-annealed (8 days) sample, and red circles: anisotropic diffusion control (ADC)-controlled (8 days) sample. (b) Magnified view of (a) between 0.95 and 1.15 eV. The spectra were normalized using the area of the Si peak. The signals of C, O, and Al were detected in the EDS spectrum, and these signals were due to the carbon tape and sample stage; they did not accrue from the samples.

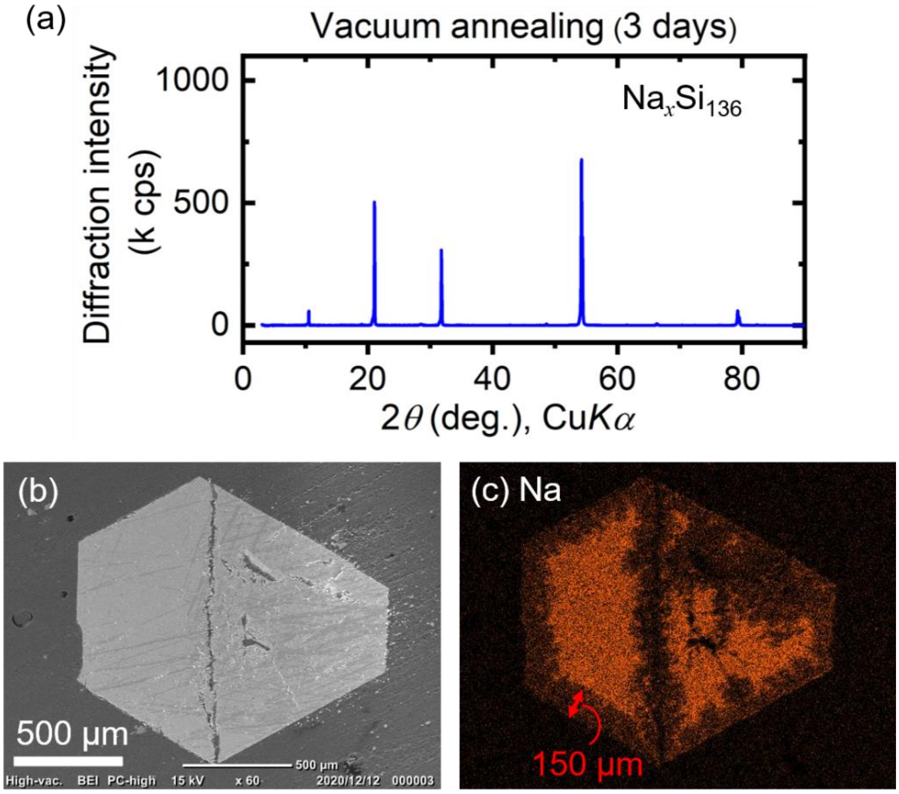

Figure S2. (a) X-ray diffraction (XRD) pattern, (b) scanning electron microscopy (SEM) image, and (c) EDS mapping of Na in the Na_xSi_{136} sample that was obtained via vacuum annealing at 450 °C for 3 days.

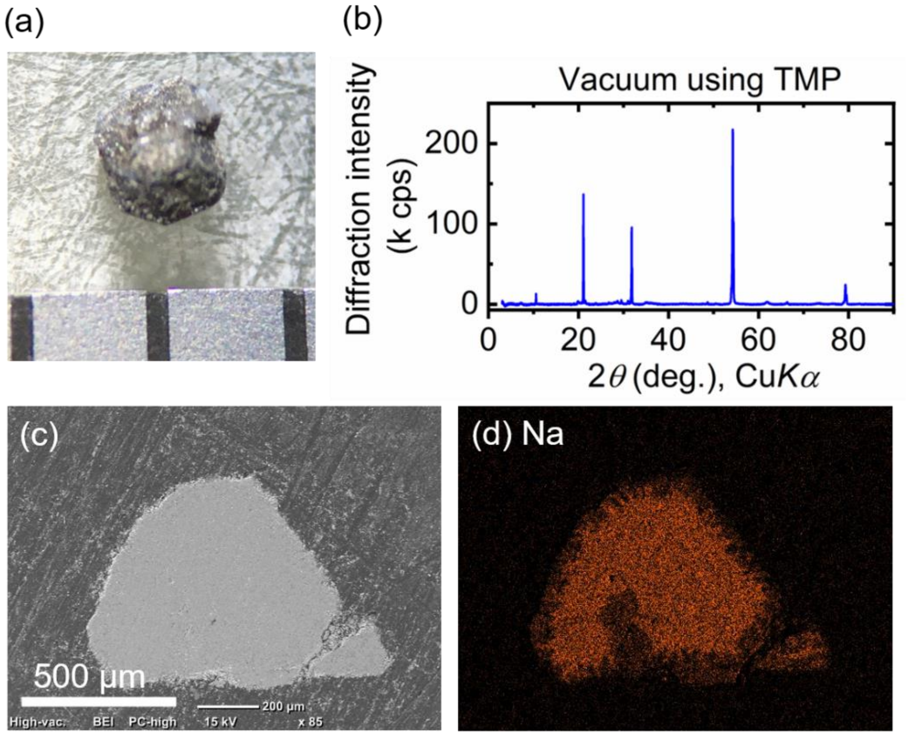

Figure S3. (a) Optical image, (b) XRD pattern, (c) SEM image, and (d) EDS mapping of Na in the Na_xSi_{136} sample that was obtained employing a turbo-molecular pump (TMP) with 3.8×10^{-6} Torr.

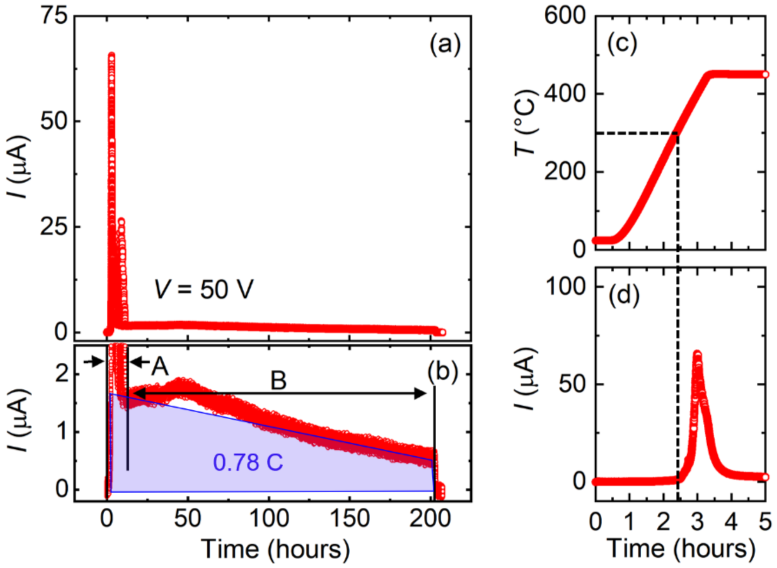

Figure S4. (a) Dependence of the electrical current (*I*) on time during the ADC process at *V* = 50 V. (b) Magnified view of (a) between 0 and 2.5 μA. (c and d) Magnified views of the temperature (*T*) and *I* between 0 and 5 h. (A) DC polarization occurred between 0 and 15 h, and (B) Na^+ migrated from the sample to NASICON between 15 and 200 h. A and B correspond to those in Figure 4(a). The final product is shown in Figure S5.

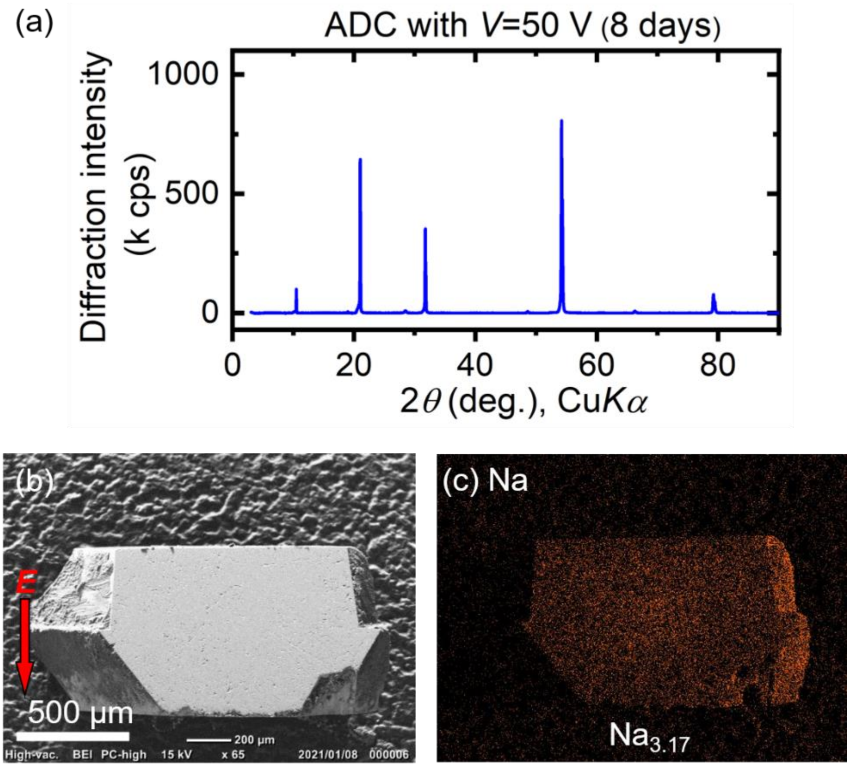

Figure S5. (a) XRD pattern, (b) SEM image, and (c) EDS mapping of Na in the Na_xSi_{136} sample, used for the ρ-T measurement, which was obtained via ADC at V = 50 V at 450 °C for 8 days. The amounts of Na in Na_xSi_{136} are indicated at the bottom in (c).

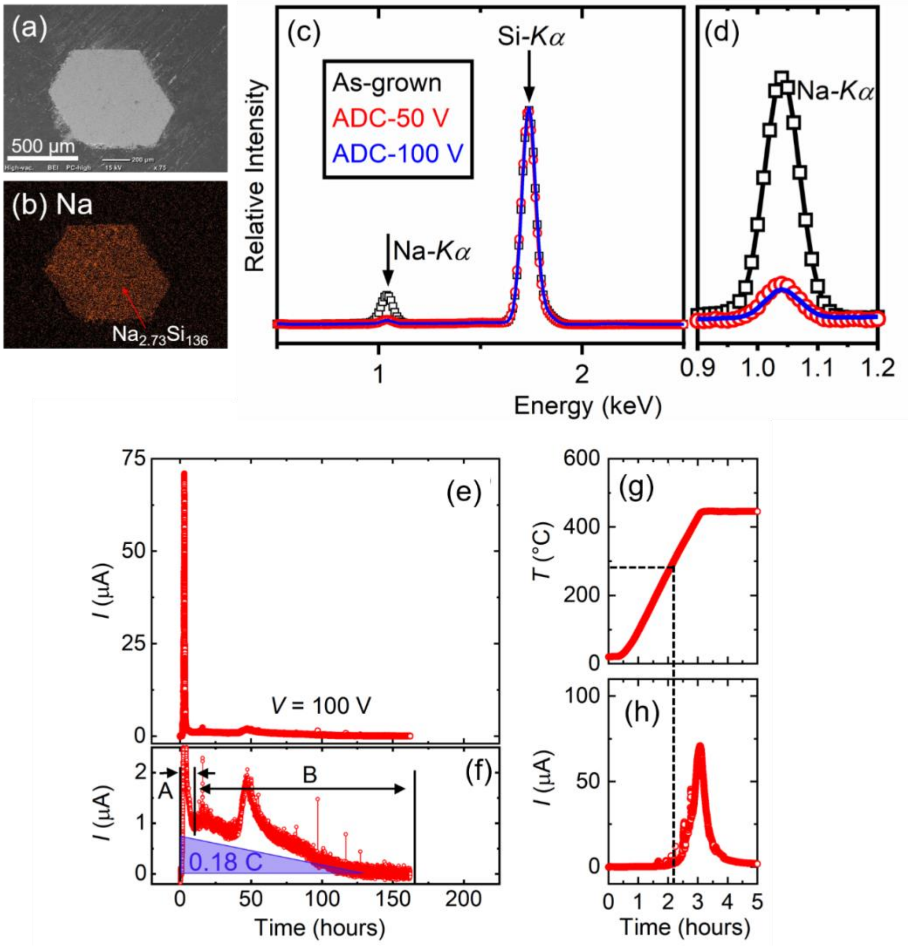

Figure S6. (a) SEM image, and (b) EDS mapping of Na in the Na$_x$Si$_{136}$ sample that was obtained via ADC at V = 100 V. (c) Comparison of the EDS spectra. Black squares: as-grown sample, red circles: ADC with 50 V, and the blue line: ADC with 100 V. The spectra were normalized with the area of the Si peak. (d) Magnified view of (c) between 0.9 and 1.2 keV. (e) Dependence of the electrical current (I) on time during the ADC process at V = 100 V. (f) Magnified view of (e) between 0 and 2.5 µA. (g and h) Magnified views of the temperature (T) and I between 0 and 5 h.

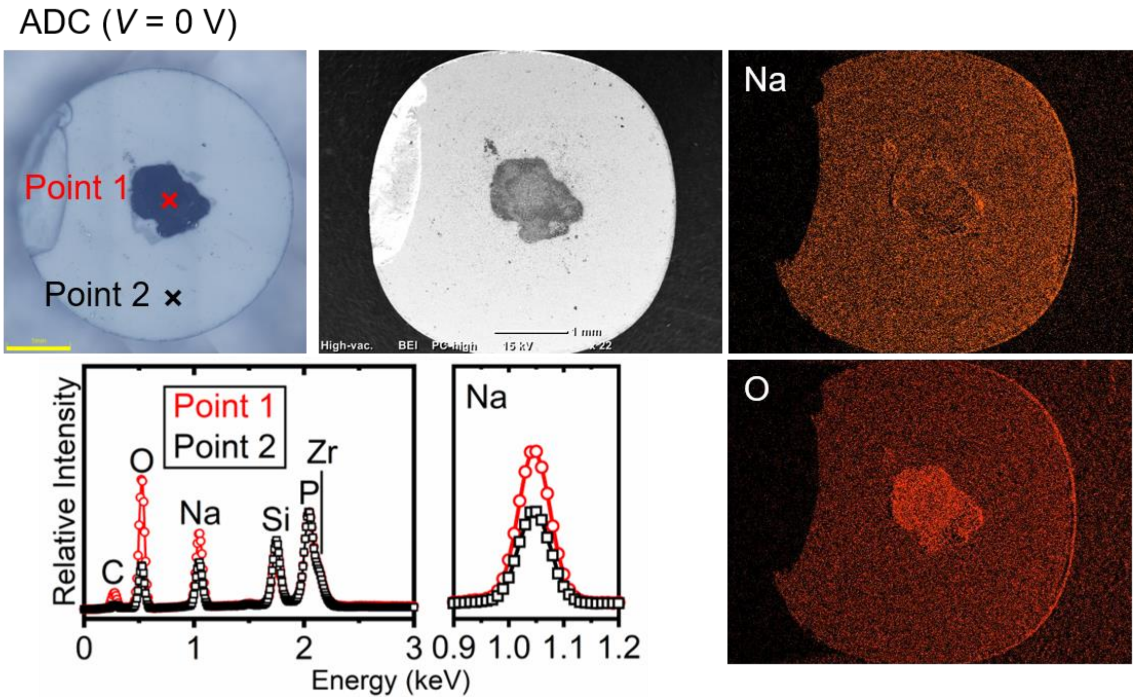

Figure S7. Optical microscopy image, SEM image, EDS mappings of Na and O, and the EDS spectra of the NASICON pellets that were utilized for the annealing with the ADC setup (V = 0 V). The EDS spectra are normalized by the area of the Si peak. A dark precipitate was observed on the NASICON pellets. The EDS spectra indicated that the precipitate comprised Na, C, and O.

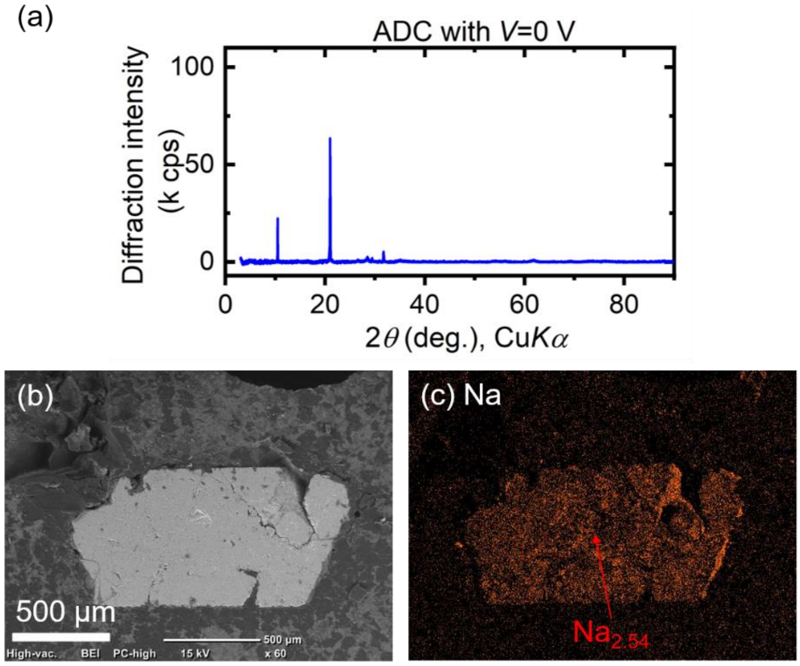

Figure S8. (a) XRD pattern, (b) SEM image, and (c) EDS mapping of Na in the Na_xSi_{136} sample that was obtained via annealing employing the ADC setup (*V* = 0 V) at 450 °C for 8 days. The amount of Na in Na_xSi_{136} is indicated at the bottom in (c).

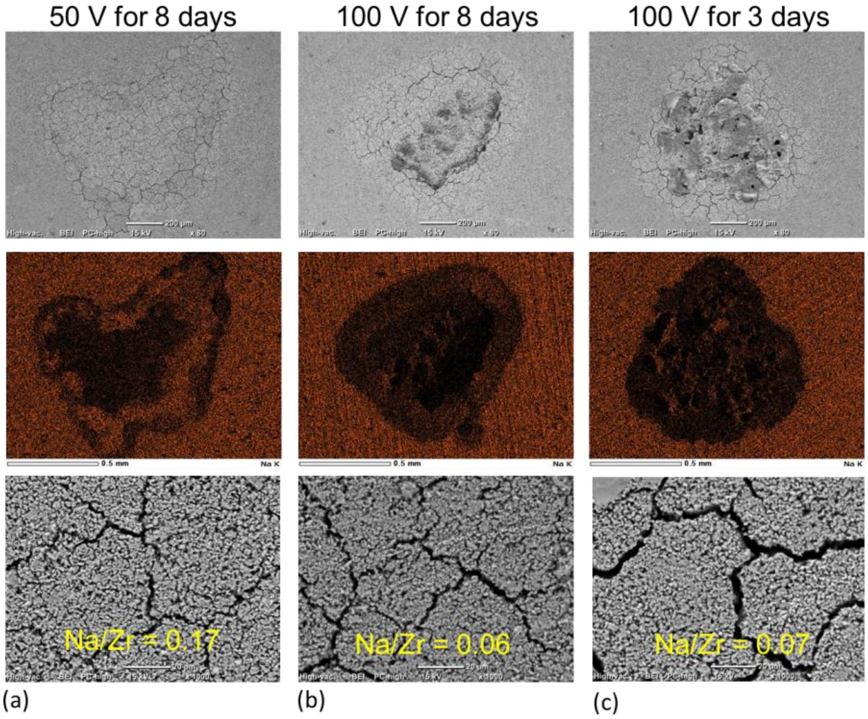

Figure S9. SEM images and EDS mappings of the surface of the Na-deficient areas: (a) 50 V for 8 days, (b) 100 V for 8 days, and (c) 100 V for 3 days.

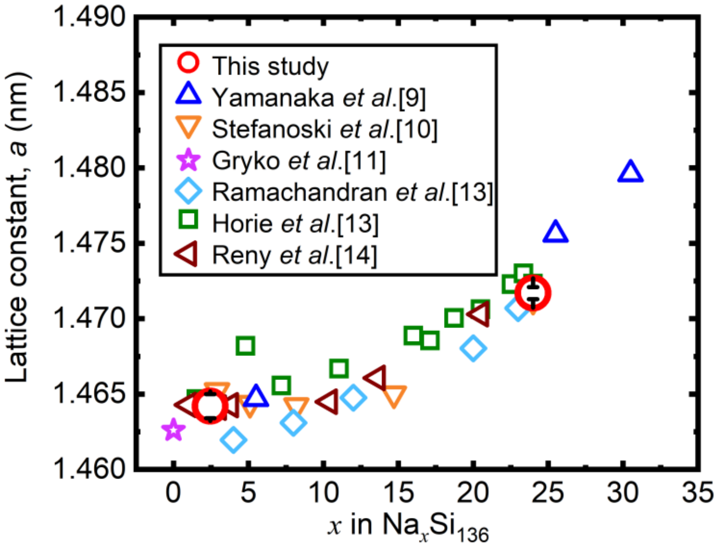

Figure S10. Lattice constant a against x in Na_xSi_{136}. The values obtained in this study are indicated by the red circles on a plot of those of the studies previously reported.[9–11, 13, 14]

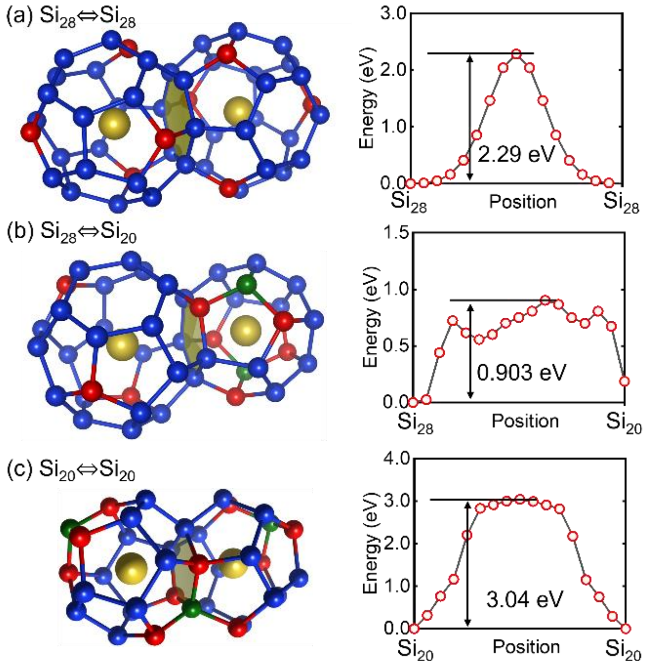

Figure S11. Three migration cases in the model without defects. The migration between (a) "Si$_{28}$–Si$_{28}$," (b) "Si$_{28}$–Si$_{20}$," or (c) "Si$_{20}$–Si$_{20}$." The highlighted planes indicate the surfaces that were sheared by the two cages. The figures on the right show the energies along the migration paths when a Na$^+$ moves from one cage to another vacant cage through the highlighted planes. The crystal structures were drawn using VESTA.[7]

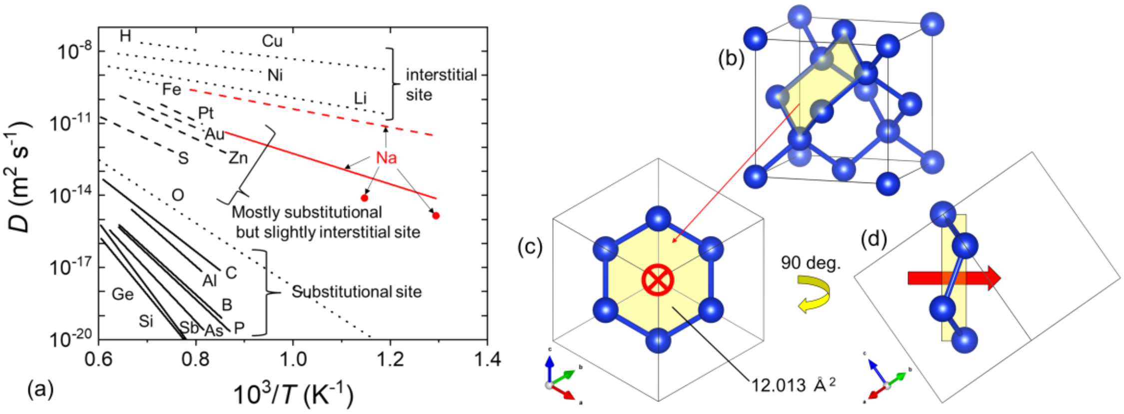

Figure S12. (a) Diffusion coefficient of various impurity atoms in diamond-structured Si. [29] (b) Crystal structure of d-Si. (c) Hexagonal plane in the crystal structure of d-Si. (d)Side view of the hexagonal plane.

Generally speaking, in the "interstitial mechanism," the diffusible atoms are small enough to occupy and can jump from one interstitial site to another. This mechanism can achieve relatively fast ion diffusion. However, as the ionic radius of diffusible atoms increases, they can not enter the interstitial site and have to be placed at a substitutional site. Then, the mechanism changes to "vacancy mechanism" or "indirect interstitial mechanism": these diffusions are performed through a substitutional site, and the ion diffusion coefficient becomes extremely small.

Figure S12(a) shows the diffusion coefficient for various impurity atoms in diamond-structured Si (d-Si). Dotted and solid lines indicate the interstitial and vacancy diffusion, respectively. Although the diffusions for Pt, Au, Zn, and S indicated by dashed lines are explained by the hybrid of both mechanisms, their atoms are mostly placed at the substitutional site. Previously reported experimental data of diffusion coefficients for Na in d-Si were added to Figure S12(a), highlighted by red. It found that the Na diffusion is thought to be categorized in the hybrid region. This means Na diffusion in d-Si may be partially accompanied by the formation of Si defects.

In addition, Figure S12(b) shows the crystal structure of d-Si. The highlighted surface by yellow is formed by six Si atoms. In the case of interstitial diffusion, ions should migrate through this surface to the next interstitial site along the arrows shown in Figures S12(c) and S12(d). Also, the area of the hexagonal plane projected on this surface can be estimated to be 12.013 Å^2. This area is much larger than pentagonal planes (9.7906 Å^2 and 9.7586 Å^2) composing Si_{20} in $Na_{24}Si_{136}$. Therefore, the Na ions in Si_{20} are more difficult to diffuse through the pentagonal plane to the interstitial site without vacancy and are more likely to require Si defect for Na diffusion than the case of d-Si. So we considered that the diffusion through the Si defect is reasonable even in the case of Si clathrate. In addition, this is the only model at the current stage that explains the experimental results of site selectivity for Na extraction of $Na_{24}Si_{136}$.

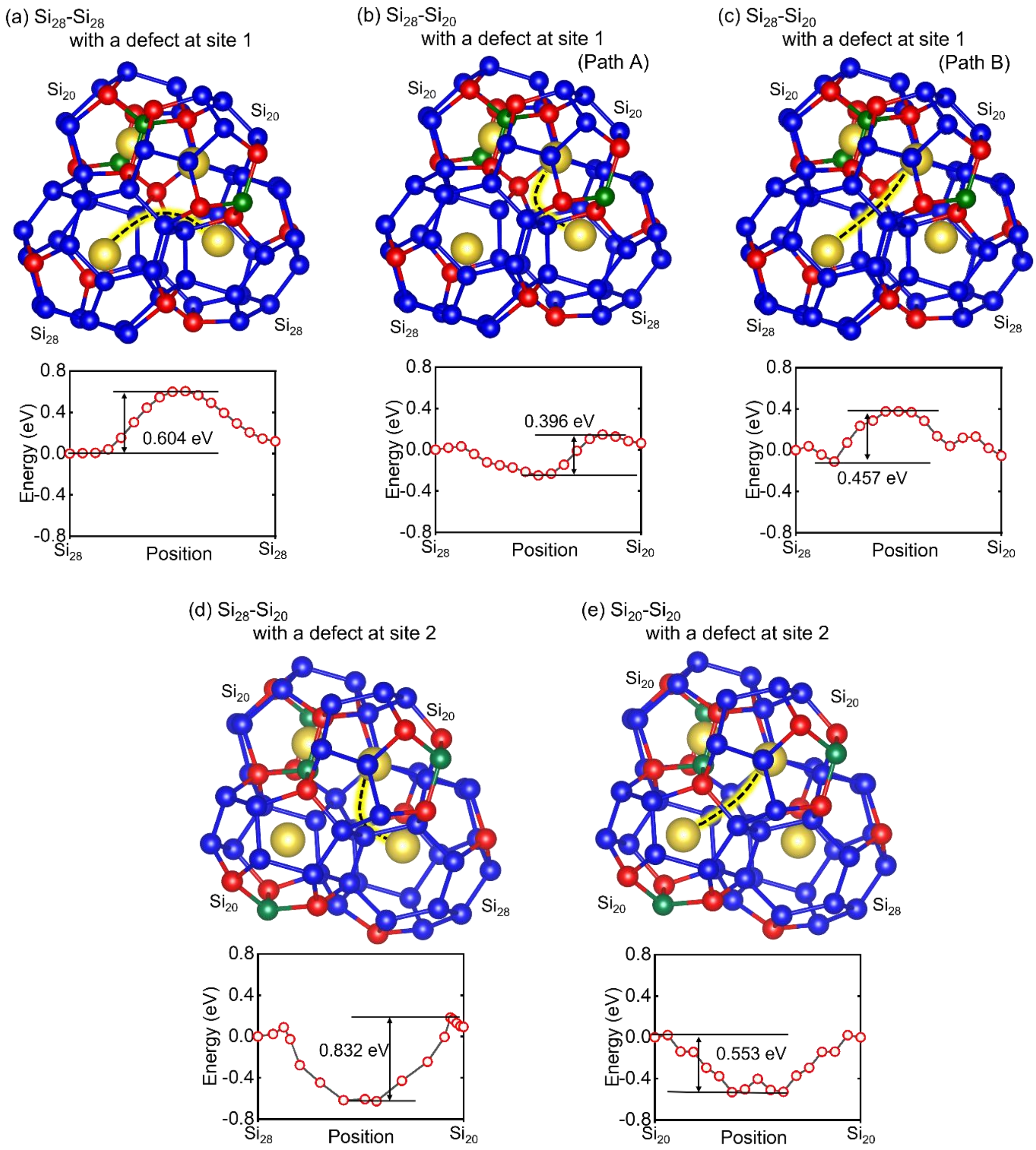

Figure S13. Four cages around a Si atom defect. The migration paths are highlighted, and the energies along the migration paths are indicated in the bottom figures. The crystal structures were drawn using VESTA.[7]

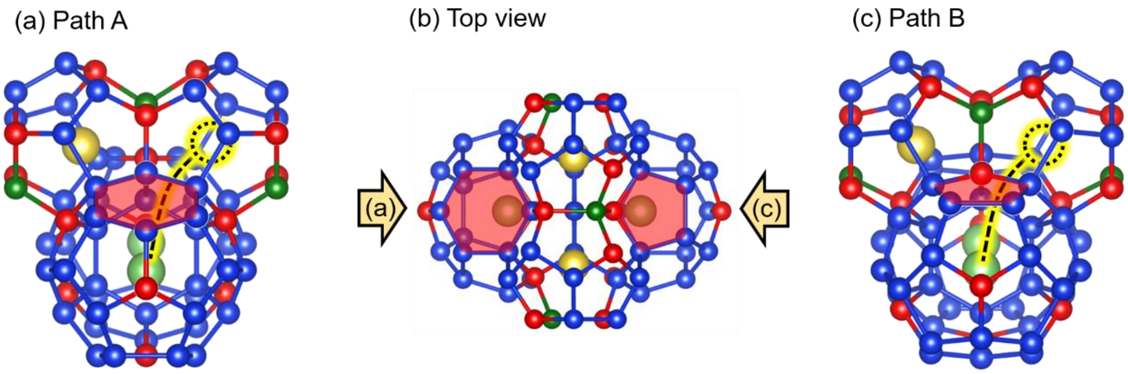

Figure S14. Schematic illustrations of (a) Path A, (b) its top view, and (c) Path B in the case of the migration between Si_{20} and Si_{28}. Path A: passing near the hexagonal plane, Path B: passing near the pentagonal plane. The crystal structures were drawn using VESTA.[7]